Geophysical Research Letters

Supporting Information for

Frictional properties and permeability variations of fault zones in the Opalinus Clay formation, a host-rock for deep nuclear waste storage.

Luis Felipe Orellana[1], Carolina Giorgetti[1], and Marie Violay[1]

[1] Laboratory of Experimental Rock Mechanics (LEMR), IIC-ENAC, École Polytechnique Fédérale de Lausanne, Lausanne, Switzerland.

Corresponding author: Luis Felipe Orellana (felipe.orellana@epfl.ch)

Contents of this file:

1. Samples, methods and data processing

1.1. Samples

We have used simulated fault gouge samples of grain sizes of less than 125 μm. were prepared from non-deformed Opalinus Clay. The mineral composition of the Opalinus clay samples consists of a major proportion of phyllosilicates (~51%), quartz (~23%), calcite (~14%), and pyrite (~1.4%). Among their constitutive phyllosilicates, kaolinite, mica, and illite-smectite are the main component totalizing ~28%, ~10%, and ~9% of the total weight content respectively (Orellana et al., 2018).

The experimental samples have been first crushed and then sieved to ensure grain sizes of less than 125 μm. Using a Malvern Mastersizer S equipment (Powder Technology Laboratory, EPFL), we have measured an average particle diameter of about 7 μm and maximum sizes of 125 μm.

1.2. Experimental setup

The frictional sliding experiments have been performed in a servo-controlled triaxial apparatus using a saw-cut configuration (Fig. S1). The triaxial apparatus is controlled by a digital controller series PCS8000 integrated with PC running the testing software DION7 (Walter + Bai AG). Axial load up to 2000 kN (accuracy of 0.01 kN) can be controlled using a displacement or force feedback loop. The triaxial apparatus can control and produce confining pressures up to 1000 bar (maximum error 0.02%). Two digital transducers are used to control and measure displacement.

The saw-cut configuration comprises two cylindrical stainless steel piston of 38 mm in diameter were cut along a plane oriented at an angle of 30° to the cylindrical axis. The saw-cut surface of each piston is characterized by a roughness (R_a) of 12.5 μm. During testing, the

pistons are separated by ~1 mm-thick layer of dry or wet powdered gouge along the saw cut. Before putting the piston assembly into the Hoek Cell, we have used a latex membrane (VJT/0554, Sols Mesures) and a rubber sealing sleeve (model 45-D0554/1, Controls Group) to act as an effective seal and to separate the specimen from the confining oil respectively. In between the latex membrane and the rubber sealing, we put anti-friction coating to reduce artificial frictional resistance. The contribution of the latex to the shear strength is found to be negligible for the 2.8 of total axial displacement.

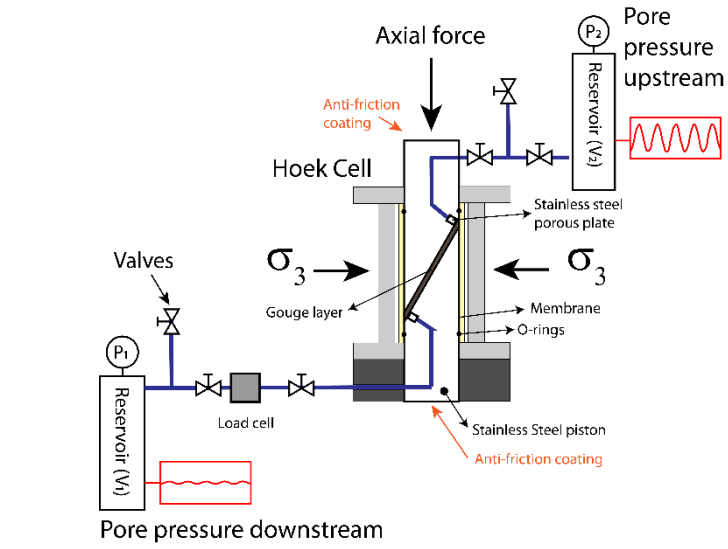

Figure 1A: Experimental setup.

At each end of the piston assembly, one sintered porous stainless steel filters of 3.8 mm in diameter (AISI 316L, GKN Sinter Metals) and 5 mm in height was placed to allow fluid flow. To measure the upstream (P_{p1}) and downstream (P_{p2}) pore fluid pressure, we have used two GDS pressure/volume controllers and the GDSLAB control and data acquisition software. Pressure and volume can go up to 16/32 MPa and 200.000 mm^3 respectively. Variations in pressure and volume were also measure using and additional sensors (Temposonics® R-Series V RP Profinet RT & IRT, resolution 0.5 µm) connected to the pore fluid pumps, which are synchronized with the controlling PC of the triaxial apparatus. The stiffness of the press and the testing setup is 626.9 kN/mm.

1.3. Testing procedure

A series of experiments (20 in total) was designed to investigate the frictional properties of dry and wet Opalinus Clay, and the evolution of permeability with fault slip. We have performed the experiments as follows:

i. We measured 5 g of dry powdered Opalinus clay that we have observed guaranteed a continuous ~1 mm-thick clay layer at the end of each experiment. For dry experiments, simulated fault gouge is first dried overnight (48 h) at 50° to avoid damage to clay mineral grains (Rutter & Mecklenburgh, 2018). The sample is kept after in a glass desiccator for at least 48 h more. For wet experiments, the dried powdered sample is mixed with ~2.5 ml of deionized water to make a paste (Lockner et al., 2011; Morrow et al., 1982; Tembe et al., 2010). The sample is then spread onto the saw cut surface of the lower piston and sandwiched by the upper stainless steel piston. Next, the sample/piston assembly is put into the membranes and Hoek Cell. Finally, we have emplaced the assembly in the triaxial apparatus and covered the top piston – triaxial apparatus contact with anti-friction coating (MoS_2.based coating).

ii. Frictional experiments on both wet and dry samples have been carried out at constant effective normal stress (σ_n) ranging from 4 to 20 MPa and at room temperature. To keep normal stress constant during sliding, we adjusted under computer control the confining pressure. For dry experiments, the assembly is loaded at 0.01 MPa/s to the target value in axial and confining pressure. Before shearing, dry samples were compacted for about 45 -60 minutes to an initial steady-state thickness. For wet experiments, hydraulic circuits were saturated with deaerated and demineralized water. Then the sample was repeatedly loaded in axial and confining pressure at 0.01 MPa/s to the desire test value. We have increased pore pressure at a rate of 0.01 MPa/s and we fixed it to 10 MPa. Once target normal stress and pore pressure were achieved, we wait for consolidation, pore pressure and volume equilibrium in both controllers (Morrow et al., 2017). This stage has lasted for at least 48 h.

iii. After pore pressures and water volume have reached equilibrium, the initial permeability (k_i) of each wet sample was measured using the oscillatory method (Bernabé et al., 2006) as a function of effective hydrostatic confining pressure (Crawford et al., 2008; Faulkner & Rutter, 2000; Rutter & Mecklenburgh, 2018; Sanchez-Roa et al., 2017). The permeability test lasted for about 10 to 12 h. Shearing did not start immediately as we have to wait for at least 12 h for re-establishing pore volumes equilibrium.

iv. Each experiment has followed a common displacement history. The initial axial loading rate for the first 2.0 mm was 1 μm/s, i.e., sliding velocity of 1.14 μm/s and strain rate of $\gamma \approx 0.001$ s-1 along the fault. After 2.0 mm of displacement, the samples were subjected to a sequence of increasing velocity-steps: 0.01-0.1, 0.1-1, and 1-10 μm/s for 0.2 mm each. These rates are slow enough to ensure controlled pore fluid pressure and, if occur, acceptable overpressures (Faulkner et al., 2018; Morrow et al., 2017). In each

step, velocity is suddenly increase inducing an instantaneous reaction in friction followed by a decay over a critical slip distance (D_c) to a new stable value of frictional strength (Scholz, 2002).

v. In wet experiments, while keeping Pp constant, we have estimated shear-enhanced compaction or dilation by measuring the volume of expelled or absorbed water respectively (Behnsen & Faulkner, 2012; French et al., 2015). Here, pore volume changes are very small (1 to 3 mm^3), thus some small fluctuations might be associated to room temperature variations. Leaks were not detected in the experiments reported here. The shearing stage last approximately 7 h.

vi. Finally, once the shearing stage was finished, we have waited 12 h again to re-establish pore volumes equilibrium. Then, we have measured end permeability (k_f) as described in point iii).

vii. Full dry test lasts around 8 to 9 hours, including sample preparation and compaction. Each wet tests have lasted at least 120 days (5 days).

1.4. Data processing

1.4.1 Friction and coefficient of friction

We have calculated friction (μ) as:

$$\mu = \frac{\tau}{\sigma_n'} = \frac{\tau}{\sigma_n - Pp} \quad (1)$$

Where τ corresponds to the shear strength parallel to the fault, σ_n the normal stress, Pp is the pore pressure, and σ_n' the effective normal stress. Shear strength (τ) was corrected for the decreasing contact area. Friction (μ) values were obtained at 2 mm of axial displacement, before velocity-steps started (Fig. 2B). In addition, we have evaluated the coefficient of friction (μ_f) and an inherent shear strength or equivalent cohesion (S_o) (Jaeger et al., 2007). Here μ_f

is the best-fit to the tangent of the $\tau - \sigma_n{}'$ curve. The values of friction μ and coefficient of friction μ_f are related as:

$$\mu = \frac{\tau}{\sigma_n{}'} = \frac{\tau}{\sigma_n - Pp} = \frac{S_o}{\sigma_n - Pp} + \mu_f \tag{2}$$

1.4.2. Frictional stability

To understand fault stability, we have computed the velocity dependence of friction via the frictional stability parameter $(a - b)$. To do that, we modelled each velocity-step using the empirical Ruina's slip –dependent evolution law, also known as Slip law (Ruina, 1983), through a least square numerical fitting routine (Noda & Shimamoto, 2009):

$$\mu = \mu_o + a \cdot ln\left(\frac{V}{V_o}\right) + b \cdot ln\left(\frac{V_o \cdot \theta}{D_c}\right), \tag{3}$$

$$\frac{d\theta}{dt} = -\frac{V \cdot \theta}{D_c} \cdot ln\left(\frac{V_o \cdot \theta}{D_c}\right)$$

Where μ_o is a constant that represents friction at steady-state for a reference velocity V_o, μ is the friction at the new steady-state velocity V, D_c the critical slip distance, and θ the average lifetime of contacts (Dieterich, 1979; Rabinowicz, 1951; Ruina, 1983; Scholz, 2002). Ruina's empirical law allows the calculation of the direct (a) and evolution (b) dimensionless constants. Thus, the computation of the frictional parameter $(a - b)$ is as follows:

$$a - b = \frac{\Delta\mu_{ss}}{ln\left(\frac{V}{V_o}\right)} \cdot \tag{4}$$

In equation (5), $\Delta\mu_{ss}$ is the change in the steady-state friction upon an immediate change in sliding velocity from V_o to V (Marone, 1998; Scholz, 2002). When $(a - b) \geq 0$ fault slip occurs in a stable manner, i.e., velocity-strengthening behavior. If $(a - b) < 0$ fault slip will potentially develop in an unstable fashion, i.e., velocity-weakening behavior (Jaeger et al.,

2007; Scholz, 2002). If necessary, we have removed the linear strengthening assuming that the strengthening is independent of the velocity-dependence of friction (Samuelson et al., 2009). When stick-slip behavior occurs, magnitudes of $(a-b)$ cannot be directly computed. Thus, we have implied velocity-weakening and calculated average stress drops $(\Delta\tau)$.

Unfortunately, our setup does not account for onboard LVDT system or equivalent to accurately measure changes in displacement close to the fault and thus stick-slip velocities during stick-slip cycles (Kaproth & Marone, 2013; Leeman et al., 2016; Scuderi et al., 2016).

1.4.2. Permeability

As indicated before, we have estimated permeability (k), before (k_i) and after (k_f) shearing, using the oscillatory method (Fischer, 1992) (Bernabé et al., 2006). Permeability was measured at a target normal stress before shearing after pore pressures and volumes were equilibrated. At the end of each shear test and to preserve the shear microstructures, we have removed shear stress and we have held normal stress constant (Rutter & Mecklenburgh, 2018). The oscillatory permeability method has been previously used in the triaxial saw-cut configuration for low permeability clays materials (Crawford et al., 2008; Faulkner & Rutter, 1998, 2000; Rutter & Mecklenburgh, 2018; Sanchez-Roa et al., 2017).

The oscillatory method is based on the transmission of a pore pressure wave within the porous media. The method applies a sinusoidal pore-fluid pressure oscillation in the up-stream reservoir using a servo-controlled pump. The amplitude and period of the imposed oscillation were fixed to 1 MPa and 1800 s, respectively. The resulting pressure variations are recorded in the downstream reservoir in terms of phase shift θ and amplitude ratio A. Two dimensionless parameters storativity (ξ) and permeability (η), are calculated as:

$$\xi = \frac{S \cdot L \cdot \beta}{\beta_d} \qquad \eta = \frac{A' \cdot t \cdot k}{\pi \cdot L \cdot \mu_{vis} \cdot \beta_d} \tag{5}$$

Where A' is the cross-sectional area of the sample, L is the length or height of the sample, β is the unknown sample storage capacity, β_d is the downstream reservoir compressibility, t the period of the upstream excitation, k the permeability of the formation and μ_{vis} the dynamic viscosity of the pore fluid. In various tests, the storage capacity of the samples could not be determined accurately across the whole pressure range by the oscillation method employed here. These data must be then interpreted with caution. The relation between parameters ξ and η, and the measured values of θ and A is given by:

$$Ae^{-i\theta} = \left(\frac{1+i}{\sqrt{\xi\eta}} \sinh\left[(1+i)\sqrt{\frac{\xi}{\eta}} \right] + \cosh\left[(1+i)\sqrt{\frac{\xi}{\eta}} \right] \right)^{-1} \quad (6)$$

Further details on the technique and the processing of the signal can be found in Bernabé et al., (2006).

2. Results

Table 1A. Results for wet tests of the numerical fitting of the empirical constants a, b, and Dc. Measurements of permeability before (k_i) and after (k_f) shearing.

Test	Normal stress σ_n [MPa]	Condition	Friction μ at 2 mm	Permeability k [m2]		Axial Velocity [μm/s]	a-b	D_c [μm]
				Before k_i	After k_f			
t006	4	wet	0.41	n/a	n/a	0.1		10.1
						1	0.009	10.3
						10	0.012	9.9
t010	4	wet	0.25	2.0E-20	2.7E-20	0.1	0.013	10.0
						1	0.011	33.4
						10	0.012	24.3
t008	7	wet	0.32	1.9E-20	3.9E-20	0.1	0.006	4.0
						1	0.008	38.7
						10	0.008	10.1
t024	7	wet	0.27	7.6E-21	3.3E-20	0.1	0.002	7.5
						1	0.005	10.5
						10	0.007	24.2
t007	10	wet	0.23	1.1E-20	2.4E-20	0.1	0.006	38.8
						1	0.007	44.1
						10	0.004	34.6
t016	10	wet	0.21	6.7E-21	2.0E-20	0.1	0.005	38.8
						1	0.005	21.7
						10	0.007	34.5
t009	20	wet	0.18	6.2E-21	1.8E-20	0.1	0.004	1.1
						1	0.005	15.1
						10	0.005	9.5
t025	20	wet	0.21	7.5E-21	1.7E-20	0.1	0.004	1.6
						1	0.005	31.1
						10	0.005	37.5

Table 2A. Results for dry tests of the numerical fitting of the empirical constants a, b, and Dc. Measurements of average stress drop $\Delta\tau$ and recurrence time t_r or all dry experiments

Test	Normal stress σ_n [MPa]	Condition	Friction μ at 2 mm	Axial Velocity [μm/s]	a-b	D_c [μm]	# SS events	Average $\Delta\tau$ [Mpa]	Average t_r [s]
t001	4	dry	0.3997	0.01	-	-	170	0.24	113.59
				0.1	-	-	197	0.16	10.08
				1	-	-	191	0.05	1.02
				10	0.004	86.21	-	-	-
t015	4	dry	0.4514	0.01	-	-	197	0.20	96.44
				0.1	-	-	236	0.15	8.44
				1	-	-	205	0.08	0.96
				10	0.001	28.627	-	-	-
t020	7	dry	0.4169	0.01	-	-	189	0.26	101.87
				0.1	-	-	195	0.25	10.26
				1	-	-	134	0.17	1.46
				10	0.003	0.019571	-	-	-
t005	7	dry	0.395	0.01	-	-	177	0.21	110.17
				0.1	-	-	226	0.18	8.86
				1	-	-	194	0.12	1.02
				10	0.008	168.53	-	-	-
t014	7	dry	0.4006	0.01	-	-	196	0.23	103.93
				0.1	-	-	244	0.22	8.16
				1	-	-	208	0.14	0.95
				10	0.002	0.10569	-	-	-
t021	10	dry	0.4081	0.01	-	-	166	0.56	118.20
				0.1	-	-	129	0.27	15.31
				1	-	-	-	-	-
				10	0.003	2123.1	-	-	-
t002	10	dry	0.3321	0.01	-	-	191	0.20	100.87
				0.1	-	-	215	0.19	9.19
				1	-	-	181	0.17	1.10
				10	0.0033	10.71	-	-	-
t012	10	dry	0.375	0.01	-	-	184	0.25	105.57
				0.1	-	-	213	0.26	8.38
				1	-	-	165	0.21	1.21
				10	0.0056	0.98	-	-	-
t018	10	dry	0.372	0.01	-	-	181	0.25	107.79
				0.1	-	-	225	0.24	8.86
				1	-	-	161	0.18	1.22
				10	n/a	n/a	-	-	-
t023	20	dry	0.3815	0.01	-	-	126	0.33	145.22
				0.1	-	-	159	0.31	12.51
				1	-	-	117	0.18	1.69
				10	0.0039	94.83	-	-	-
t017	20	dry	0.3678	0.01	-	-	145	0.23	130.71
				0.1	-	-	206	0.33	9.64
				1	-	-	118	0.40	1.67
				10	0.0052	1154.10	-	-	-

3. References

Bernabé, Y., Mok, U., & Evans, B. (2006). A note on the oscillating flow method for measuring rock permeability. *International Journal of Rock Mechanics and Mining Sciences*, *43*(2), 311–316. https://doi.org/10.1016/j.ijrmms.2005.04.013

Crawford, B. R., Faulkner, D., & Rutter, E. (2008). Strength, porosity, and permeability development during hydrostatic and shear loading of synthetic quartz-clay fault gouge. *Journal of Geophysical Research: Solid Earth*, *113*(3), 1–14. https://doi.org/10.1029/2006JB004634

Dieterich, J. H. (1979). Modeling of rock friction: 1. Experimental results and constituve equations. *Journal of Geophysical Research*, *84*(9), 2161–2168. https://doi.org/10.1007/BF00876539

Faulkner, D., & Rutter, E. (1998). The gas permeability of clay-bearing fault gouge at 20°C. *Geological Society, London, Special Publications*, *147*(1), 147–156. https://doi.org/10.1144/GSL.SP.1998.147.01.10

Faulkner, D., & Rutter, E. (2000). Comparisons of water and argon permeability in natural clay-bearing fault gouge under high pressure at 20°C. *Journal of Geophysical Research*, *105*(B7), 16415. https://doi.org/10.1029/2000JB900134

Faulkner, D., Sanchez-Roa, C., Boulton, C., & Den Hartog, S. A. M. (2018). Pore Fluid Pressure Development in Compacting Fault Gouge in Theory, Experiments, and Nature. *Journal of Geophysical Research: Solid Earth*, *123*(1), 226–241. https://doi.org/10.1002/2017JB015130

Fischer, G. J. (1992). The determination of permeability and storage capacity: Pore pressure oscillation method. In B. Evans & T.-F. Wong (Eds.), *Fault mechanics and transport properties of rocks* (pp. 187–212). New York: Academic Press.

Jaeger, J., Cook, N. G., & Zimmerman, R. (2007). *Fundamentals of Rock Mechanics, 4th Edition* (4th Editio). Blackwell Publising.

Kaproth, B., & Marone, C. (2013). Slow earthquakes, preseismic velocity changes, and the origin of slow frictional stick-slip. *Science*, *341*(6151), 1229–1232. https://doi.org/10.1126/science.1239577

Leeman, J., Saffer, D., Scuderi, M. M., & Marone, C. (2016). Laboratory observations of slow earthquakes and the spectrum of tectonic fault slip modes. *Nature Communications*, *7*, 1–6. https://doi.org/10.1038/ncomms11104

Lockner, D. A., Morrow, C., Moore, D., & Hickman, S. (2011). Low strength of deep San Andreas fault gouge from SAFOD core. *Nature*, *472*(7341), 82–86. https://doi.org/10.1038/nature09927

Marone, C. (1998). Laboratory-Derived Friction Laws and Their Application To Seismic Faulting. *Annual Review of Earth and Planetary Sciences*, *26*(1), 643–696. https://doi.org/10.1146/annurev.earth.26.1.643

Morrow, C., Shi, L. Q., & Byerlee, J. D. (1982). Strain hardening and strength of clay-rich fault

gouges. *Journal of Geophysical Research*, *87*(B8), 6771–6780. https://doi.org/10.1029/JB087iB08p06771

Morrow, C., Moore, D., & Lockner, D. A. (2017). Frictional strength of wet and dry montmorillonite. *Journal of Geophysical Research: Solid Earth*, *122*(5), 3392–3409. https://doi.org/10.1002/2016JB013658

Noda, H., & Shimamoto, T. (2009). Constitutive properties of clayey fault gouge from the Hanaore fault zone, southwest Japan. *Journal of Geophysical Research: Solid Earth*, *114*(4), 1–29. https://doi.org/10.1029/2008JB005683

Orellana, L. F., Scuderi, M. M., Collettini, C., & Violay, M. (2018). Frictional Properties of Opalinus Clay: Implications for Nuclear Waste Storage. *Journal of Geophysical Research: Solid Earth*, *123*(1), 157–175. https://doi.org/10.1002/2017JB014931

Rabinowicz, E. (1951). The nature of the static and kinetic coefficients of friction. *Journal of Applied Physics*, *22*(11), 1373–1379. https://doi.org/10.1063/1.1699869

Ruina, A. (1983). Slip instability and state variable friction laws. *Journal of Geophysical Research*, *88*(B12), 10359. https://doi.org/10.1029/JB088iB12p10359

Rutter, E., & Mecklenburgh, J. (2018). Influence of Normal and Shear Stress on the Hydraulic Transmissivity of Thin Cracks in a Tight Quartz Sandstone, a Granite, and a Shale. *Journal of Geophysical Research: Solid Earth*, *123*(2), 1262–1285. https://doi.org/10.1002/2017JB014858

Samuelson, J., Elsworth, D., & Marone, C. (2009). Shear-induced dilatancy of fluid-saturated faults: Experiment and theory. *Journal of Geophysical Research: Solid Earth*, *114*(12), 1–15. https://doi.org/10.1029/2008JB006273

Sanchez-Roa, C., Faulkner, D., Boulton, C., Jimenez-Millan, J., & Nieto, F. (2017). How phyllosilicate mineral structure affects fault strength in Mg-rich fault systems. *Geophysical Research Letters*, *44*(11), 5457–5467. https://doi.org/10.1002/2017GL073055

Scholz, C. H. (2002). *The Mechanics of Earthquakes and Faulting*. Cambridge University Press. Retrieved from https://books.google.ch/books?id=JL1VM5wMbrQC

Scuderi, M. M., Marone, C., Tinti, E., Di Stefano, G., & Collettini, C. (2016). Precursory changes in seismic velocity for the spectrum of earthquake failure modes. *Nature Geoscience*, *9*(9), 695–700. https://doi.org/10.1038/ngeo2775

Tembe, S., Lockner, D. A., & Wong, T. F. (2010). Effect of clay content and mineralogy on frictional sliding behavior of simulated gouges: Binary and ternary mixtures of quartz, illite, and montmorillonite. *Journal of Geophysical Research: Solid Earth*, *115*(3), 1–22. https://doi.org/10.1029/2009JB006383